First evidence of $\psi(2S)\rightarrow\Omega^{-}\bar{\Omega}^{+}$ [*]

M. Ablikim(阿布里克木·麦迪娜)[1] J. Z. Bai(白景芝)[1] Y. Bai(白羽)[1] Y. Ban(班勇)[11] X. Cai(蔡啸)[1] H. F. Chen(陈宏芳)[17] H. S. Chen(陈和生)[1] J. C. Chen(陈江川)[1] J. Chen(陈进)[1] Y. B. Chen(陈元柏)[1] Y. P. Chu(初元萍)[1] Y. S. Dai(戴又善)[19] Z. Y. Deng(邓子艳)[1] S. X. Du(杜书先)[1a] J. Fang(方建)[1] C. D. Fu(傅成栋)[1] Y. Gao(高原宁)[15] Y. T. Gu(顾运厅)[4] Z. J. Guo(郭子敬)[16b] F. A. Harris[16] K. L. He(何康林)[1] M. He(何瑁)[13] Y. K. Heng(衡月昆)[1] H. M. Hu(胡海明)[1] T. Hussain[1c] T. Hu(胡涛)[1] G. S. Huang(黄光顺)[17] X. T. Huang(黄性涛)[13] Y. P. Huang(黄燕萍)[1] T. Hussain[1c] X. B. Ji(季晓斌)[1] X. S. Jiang(江晓山)[1] J. B. Jiao(焦健斌)[13] D. P. Jin(金大鹏)[1] S. Jin(金山)[1] G. Li(李刚)[1] H. B. Li(李海波)[1] J. Li(李金)[1] L. Li(李蕾)[1] R. Y. Li(李仁英)[1] W. D. Li(李卫东)[1] W. G. Li(李卫国)[1] X. L. Li(李晓玲)[13] X. N. Li(李小男)[1] X. Q. Li(李学潜)[10] Y. F. Liang(梁勇飞)[14] B. J. Liu(刘北江)[1] C. X. Liu(刘春秀)[1] Fang Liu(刘芳)[1] Feng Liu(刘峰)[6] H. B. Liu(刘宏邦)[4] H. M. Liu(刘怀民)[1] J. P. Liu(刘觉平)[18] Q. Liu(刘倩)[16d] R. G. Liu(刘荣光)[1] Z. A. Liu(刘振安)[1] F. Lu(吕峰)[1] G. R. Lu(鲁公儒)[5] J. G. Lu(吕军光)[1] X. L. Luo(罗成林)[9] F. C. Ma(马凤才)[8] H. L. Ma(马海龙)[1] Q. M. Ma(马秋梅)[1] M. Q. A. Malik[1c] Z. P. Mao(毛泽普)[1] X. H. Mo(莫晓虎)[1] J. Nie(聂晶)[1] S. L. Olsen[12] R. G. Ping(平荣刚)[1] J. F. Qiu(邱进发)[1] G. Rong(荣刚)[1] X. D. Ruan(阮向东)[4] L. Y. Shan(单连友)[1] L. Shang(尚雷)[1] C. P. Shen(沈成平)[16e] X. Y. Shen(沈肖雁)[1] H. Y. Sheng(盛华义)[1] S. S. Sun(孙海生)[1] S. S. Sun(孙胜森)[1] Y. Z. Sun(孙永昭)[1] Z. J. Sun(孙志嘉)[1] X. Tang(唐晓)[1] J. P. Tian(田俊平)[15] G. S. Varner[16] X. Wan(万霞)[1] L. Wang(王岚)[1] L. L. Wang(王亮亮)[1] L. S. Wang(王灵淑)[1] P. Wang(王平)[1] P. L. Wang(王佩良)[1] Y. F. Wang(王贻芳)[1] Z. Wang(王铮)[1] Z. Y. Wang(王至勇)[1] C. L. Wei(魏诚林)[1] D. H. Wei(魏代会)[3] N. Wu(吴宁)[1] G. F. Xu(许国发)[1] X. P. Xu(徐新平)[6f] Y. Xu(徐晔)[10] M. L. Yan(阎沐霖)[17] H. X. Yang(杨洪勋)[1] M. Yang(杨明)[1] Y. X. Yang(杨永栩)[3] M. H. Ye(叶铭汉)[2] Y. X. Ye(叶云秀)[17] C. X. Yu(喻纯旭)[10] C. Z. Yuan(苑长征)[1] Y. Yuan(袁野)[1] Y. Zeng(曾云)[7] B. X. Zhang(张丙新)[1] B. Y. Zhang(张炳云)[1] C. C. Zhang(张长春)[1] D. H. Zhang(张达华)[1] H. Q. Zhang(张华桥)[1] H. Y. Zhang(章红宇)[1] J. W. Zhang(张家文)[1] J. Y. Zhang(张建勇)[1] X. Y. Zhang(张学尧)[13] Y. Y.Zhang(张一云)[14] Z. P. Zhang(张子平)[17] J. W. Zhao(赵京伟)[1] M. G. Zhao(赵明刚)[10] P. P. Zhao(赵平平)[1] Z. G. Zhao(赵政国)[17] B. Zheng(郑波)[1] H. Q. Zheng(郑海青)[11] J. P. Zheng(郑建平)[1] Z. P. Zheng(郑志鹏)[1] B. Zhong(钟彬)[1] L. Zhou(周莉)[1] K. J. Zhu(朱科军)[1] Q. M. Zhu(朱启明)[1] X. W. Zhu(朱兴旺)[1] Y. S. Zhu(朱永生)[1] Z. A. Zhu(朱自安)[1] B. S. Zou(邹冰松)[1]

(BESⅡ collaboration)

[1] Institute of High Energy Physics, Beijing 100049, China
[2] China Center of Advanced Science and Technology, Beijing 100190, China
[3] Guangxi Normal University, Guilin 541004, China
[4] Guangxi University, Nanning 530004, China
[5] Henan Normal University, Xinxiang 453007, China

Received 11 July 2012, Revised 14 August 2012

* Supported by National Natural Science Foundation of China (10491300, 10225524, 10225525, 10425523, 10625524, 10521003, 10821063, 10825524), Chinese Academy of Sciences (KJ 95T-03), 100 Talents Program of CAS (U-11, U-24, U-25), Knowledge Innovation Project of CAS (U-602, U-34 (IHEP)), National Natural Science Foundation of China (10775077, 10225522) (Tsinghua University), and Department of Energy (DE-FG02-04ER41291) (U. Hawaii)

[6] Huazhong Normal University, Wuhan 430079, China
[7] Hunan University, Changsha 410082, China
[8] Liaoning University, Shenyang 110036, China
[9] Nanjing Normal University, Nanjing 210046, China
[10] Nankai University, Tianjin 300071, China
[11] Peking University, Beijing 100871, China
[12] Seoul National University, Seoul, 151-747 Korea
[13] Shandong University, Jinan 250100, China
[14] Sichuan University, Chengdu 610064, China
[15] Tsinghua University, Beijing 100084, China
[16] University of Hawaii, Honolulu, Hawaii 96822, USA
[17] University of Science and Technology of China, Hefei 230026, China
[18] Wuhan University, Wuhan 430072, China
[19] Zhejiang University, Hangzhou 310027, China
[a] now at Zhengzhou University, Zhengzhou 450001, China
[b] now at Johns Hopkins University, Baltimore, MD 21218, USA
[c] now at Centre for High Energy Physics, University of the Punjab, Lahore-54590, Pakistan
[d] now at Graduate University of Chinese Academy of Sciences, Beijing 100049, China
[e] now at Nagoya University, Nagoya, Japan
[f] now at Soochow University, Suzhou 215006, China

Abstract: The decay $\psi(2S)\rightarrow\Omega^-\bar{\Omega}^+$ is analyzed using 14×10^6 $\psi(2S)$ events recorded by the Beijing Spectrometer II (BES II) at the Beijing Electron Positron Collider (BEPC). Based upon events with no missing charged tracks and a satisfactory four-constraint kinematic fit, we determine the upper limit for the branching fraction of $\psi(2S)\rightarrow\Omega^-\bar{\Omega}^+$ to be 1.5×10^{-4} at a 90% confidence level. By including events with one missing charged track, we are able to report the first evidence of an $\Omega^-\bar{\Omega}^+$ signal with a statistical significance of 3.1σ. The branching fraction of $\psi(2S)\rightarrow\Omega^-\bar{\Omega}^+$ is determined to be $(4.80\pm1.56(\text{stat})\pm1.30(\text{sys}))\times10^{-5}$.

Key words: upper limit, first evidence, significance level, branching fraction

PACS: 14.40.Pq, 14.65.Dw, 14.20.Gk **DOI:** 10.1088/1674-1137/36/11/002

1 Introduction

The production of $\psi(2S)$ in e^+e^- annihilation and its two-body hadronic decays can be used to test the predictive power of QCD [1]. These decays occur, mainly, via $c\bar{c}$ annihilation into either three gluons or a photon [2]. The gluons or the photon may lead to baryon antibaryon production e.g., $\Omega^-\bar{\Omega}^+$. In $\psi(2S)\rightarrow\Omega^-\bar{\Omega}^+$, Ω^- and $\bar{\Omega}^+$ are produced, predominantly through hadronization of gluons into three $s\bar{s}$ quark antiquark pairs. Earlier studies of this decay mode have provided upper limits at the 90% confidence level: 7.3×10^{-5} [3] and 1.6×10^{-4} [4]. In our analysis we use 14 M $\psi(2S)$ data registered by the BES II detector, to search for $\psi(2S)\rightarrow\Omega^-\bar{\Omega}^+$ decay events. For this purpose we reconstruct the $\Omega^-(\bar{\Omega}^+)$ from $\Lambda K^-(\bar{\Lambda}K^+)$ invariant mass spectrum, where $\Lambda(\bar{\Lambda})$ is reconstructed from $p\pi^-(\bar{p}\pi^+)$ combination. An important aspect of this analysis is that it also includes events with one missing track, which increases the detection efficiency from 1.62% (for events with 6 charged tracks) to 10.17% (for events with 6 or 5 charged tracks). We report an upper limit for the branching fraction of $\psi(2S)\rightarrow\Omega^-\bar{\Omega}^+$, using events satisfying a four-constraint kinematic fit, to be 1.5×10^{-4} at the 90% confidence level. For events with one missing charged track and satisfying a one-constraint kinematic fit, we determine the branching fraction to be $(4.80\pm1.56(\text{stat})\pm1.30(\text{sys}))\times10^{-5}$ with a 3.1σ significance.

2 The BES II Detector

BES II, a large solid-angle magnetic detector, was employed at the BEPC [5]. Its innermost part, the 'vertex chamber' (VC) has twelve layers surrounding the Beryllium beam pipe. It provides track and trigger information of events. Outside the VC, there is a forty-layer 'main drift chamber' (MDC) covering 85% of the total solid angle. It measures the momentum and energy loss ($\mathrm{d}E/\mathrm{d}x$) of charged particles, with resolutions: $\sigma_p/p=1.78\%\sqrt{1+p^2}$ (p in GeV/c) and $\sigma_{\mathrm{d}E/\mathrm{d}x}\sim8\%$. A barrel-like array of forty-eight scintillation counters outside the MDC and covering 80% of the total solid-angle is employed to provide time-of-flight (TOF) information of particles with resolutions: $\sigma_{\text{TOF}}=180$ ps (for Bhabha events) and $\sigma_{\text{TOF}}=200$ ps (for hadronic events). Outside the TOF system, there is a twelve-radiation-length lead-gas 'barrel shower counter' (BSC). It measures the energy and position of electrons and photons, with resolutions: $\sigma_E/E = 21\%/\sqrt{E}$ (E in GeV), $\sigma_\phi = 7.9$ mrad, and $\sigma_z = 2.3$ cm. In the outermost part of the detector, three double layers of proportional counters are instrumented to identify muons.

The performance of the detector is checked through Monte Carlo (MC) simulations. A reasonable agreement is found between the data and MC results in high purity decay channels [6].

3 Event selection

The final state particles of $\psi(2S) \to \Omega^-\bar{\Omega}^+$ have momentum values with $p < 0.8$ GeV/c. Allowing for the possibility of missing low momentum particle(s) during the reconstruction of charged tracks, events with one missing charged track are also selected. Thus $\psi(2S)$ events with six or five charged tracks (net charge: 0 or +1 or −1) that are well reconstructed from the MDC information are selected. All charged tracks are required to have a minimum transverse momentum of 70 MeV/c and lie within the fiducial region of the MDC; $|\cos\theta| \leqslant 0.8$. As $\Omega^-(\bar{\Omega}^+)$ and Λ ($\bar{\Lambda}$) have long life-times: $(0.821\pm0.011)\times10^{-10}$ s [7] and $(2.631\pm0.020)\times10^{-10}$ s [7], respectively, charged tracks are required to satisfy only the loose vertex constraints: $R_{xy} = \sqrt{x_0^2+y_0^2} \leqslant 0.2$ m and $|R_{z0}| \leqslant 0.3$ m (x_0, y_0 and z_0 are the coordinates of the point of closest approach to the interaction point).

Particle identification is based only upon the track's dE/dx information (using time-of-flight information also, would result in comparatively low detection efficiency). The corrected dE/dx information of each charged track is used to determine χ^2 values for each of the three particle/antiparticle hypotheses:

$$\chi^2_{\mathrm{d}E/\mathrm{d}x}(i) = \left[\frac{\mathrm{d}E/\mathrm{d}x_{\mathrm{measured}} - \mathrm{d}E/\mathrm{d}x_{\mathrm{expected}}(i)}{\sigma_{\mathrm{d}E/\mathrm{d}x}(i)}\right]^2,$$

where $\mathrm{d}E/\mathrm{d}x_{\mathrm{measured}}$, $\mathrm{d}E/\mathrm{d}x_{\mathrm{expected}}(i)$ and $\sigma_{\mathrm{d}E/\mathrm{d}x}(i)$ represent the measured dE/dx, the expected dE/dx and the dE/dx resolution for a particle/antiparticle hypothesis i, respectively. For each charged track of an event, three $\chi^2_{\mathrm{d}E/\mathrm{d}x}$ values are obtained, one for each of the three particle/antiparticle hypotheses (p, π^+, K^+ or $\bar{\mathrm{p}}$, π^-, K^-). Proton (p), pion (π^+) and kaon (K^+) are identified by using, respectively, the following inequalities:

$\chi^2_{\mathrm{d}E/\mathrm{d}x}(\mathrm{p}) < \chi^2_{\mathrm{d}E/\mathrm{d}x}(\pi^+)$ and $\chi^2_{\mathrm{d}E/\mathrm{d}x}(\mathrm{p}) < \chi^2_{\mathrm{d}E/\mathrm{d}x}(\mathrm{K}^+)$,

$\chi^2_{\mathrm{d}E/\mathrm{d}x}(\pi^+) < \chi^2_{\mathrm{d}E/\mathrm{d}x}(\mathrm{p})$ and $\chi^2_{\mathrm{d}E/\mathrm{d}x}(\pi^+) < \chi^2_{\mathrm{d}E/\mathrm{d}x}(\mathrm{K}^+)$,

$\chi^2_{\mathrm{d}E/\mathrm{d}x}(\mathrm{K}^+) < \chi^2_{\mathrm{d}E/\mathrm{d}x}(\pi^+)$ and $\chi^2_{\mathrm{d}E/\mathrm{d}x}(\mathrm{K}^+) < \chi^2_{\mathrm{d}E/\mathrm{d}x}(\mathrm{p})$.

Negatively charged particles ($\bar{\mathrm{p}}$, π^- and K^-) are also identified using similar criteria. The $\chi^2_{\mathrm{d}E/\mathrm{d}x}$ distributions for the three particle/anti-particle hypotheses when a proton/anti-proton is identified, are shown in Fig. 1. The individual events have distinct values of $\chi^2_{\mathrm{d}E/\mathrm{d}x}$ for three hypotheses but for all events an overlapping between adjacent $\chi^2_{\mathrm{d}E/\mathrm{d}x}$ distributions is seen as shown in Fig. 1.

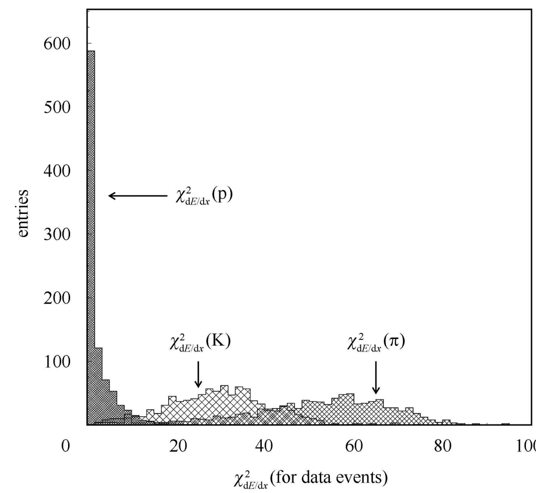

Fig. 1. The $\chi^2_{\mathrm{d}E/\mathrm{d}x}$ distributions of p, π and K hypotheses for the selected data events when p is identified.

Events with six identified particles are subjected to a four constraint (4C) kinematic fit imposing energy and momentum conservation, and those with five identified particles to a one constraint (1C) kinematic fit imposing energy conservation. Events passing the 4C kinematic fit are required to have $\chi^2_{4\mathrm{C}} < 20$, while for those passing the 1C fit, an optimized cut i.e., $\chi^2_{1\mathrm{C}} < 10$ is applied. For events passing either the 4C or 1C kinematic fit, the $\mathrm{p}\pi^-$ ($\bar{\mathrm{p}}\pi^+$) and $\Lambda\mathrm{K}^-$ ($\bar{\Lambda}\mathrm{K}^+$) invariant mass spectra are reconstructed to select Λ ($\bar{\Lambda}$) and Ω^- ($\bar{\Omega}^+$) signals. For events satisfying the 4C selection, the mass resolutions of Λ ($\bar{\Lambda}$) and Ω^- ($\bar{\Omega}^+$) signals are determined to be ≈ 3 MeV/c^2 and ≈ 5 MeV/c^2, respectively, through single Gaussian fits to the respective MC invariant mass spectra. In this case, $\Lambda(\bar{\Lambda})$ and $\Omega^-(\bar{\Omega}^+)$ mass limits are selected as $|M_{\mathrm{p}\pi^-} - M_\Lambda| < 9$ ($|M_{\bar{\mathrm{p}}\pi^+} - M_{\bar{\Lambda}}| < 9$) MeV/$c^2$ and $|M_{\Lambda\mathrm{K}^-} - M_{\Omega^-}| < 15$ ($|M_{\bar{\Lambda}\mathrm{K}^+} - M_{\bar{\Omega}^+}| < 15$) MeV/$c^2$.

For events passing the 1C selection, the mass resolutions of Λ ($\bar{\Lambda}$) and Ω^- ($\bar{\Omega}^+$) signals are determined to be ≈ 10 MeV/c^2 and ≈ 20 MeV/c^2, respectively, through double Gaussian fits to the respective MC invariant mass spectra. In this case $\Lambda(\bar{\Lambda})$ and $\Omega^-(\bar{\Omega}^+)$ asymmetric mass limits are determined for 97.3% area of the invariant mass spectra to be

$1090 < M_{p\pi^-} < 1150$ ($1090 < M_{\bar{p}\pi^+} < 1150$) MeV/$c^2$ and $1630 < M_{\Lambda K^-} < 1750$ ($1630 < M_{\bar{\Lambda}K^+} < 1750$) MeV/$c^2$.

4 The analysis results

Comparisons between $p\pi^-$ (ΛK^-) and $\bar{p}\pi^+$ ($\bar{\Lambda}K^+$) invariant mass spectra of data events are shown in Figs. 2 and 3, where the histograms represent $p\pi^-$ and ΛK^- invariant mass spectra and the dots with error bars represent $\bar{p}\pi^+$ and $\bar{\Lambda}K^+$ invariant mass spectra. Background is analyzed by using exclusive MC samples as well as a 14 million inclusive $\psi(2S)$ MC. The exclusive background channels, each with 10,000 MC events, include $\psi(2S)\to\Lambda\bar{\Lambda}\pi^+\pi^-$; $\psi(2S)\to\Lambda\bar{\Lambda}\phi(1020)$, $\phi\to K^+K^-$; $\psi(2S)\to\Xi^-\bar{\Xi}^+,\Xi^-\to\Lambda\pi^-,\bar{\Xi}^+\to\bar{\Lambda}\pi^+$; and $\psi(2S)\to\Lambda\bar{p}K^+\pi^+\pi^-$. $\psi(2S)\to\Lambda\bar{\Lambda}\phi(1020)$, with $\phi(1020)\to K^+K^-$, is found to be the main background channel. The K^+K^- invariant mass spectrum for data events is shown in Fig. 4.

From a single Gaussian fit to the MC K^+K^- invariant mass spectrum, the mass resolution (σ_ϕ) is found to be ≈ 5 MeV/c^2. The background contribution of $\psi(2S)\to\Lambda\bar{\Lambda}\phi(1020)$, with $\phi(1020)\to K^+K^-$ in the $\Omega^-\bar{\Omega}^+$ signal region for 1C selected events is removed by requiring $|M(K^+K^-)-M(\phi(1020))| > 3\times\sigma_\phi$. This requirement is applied only for 1C events in the signal region of the scatter plot of $M(\Lambda K^-)$ versus $M(\bar{\Lambda}K^+)$.

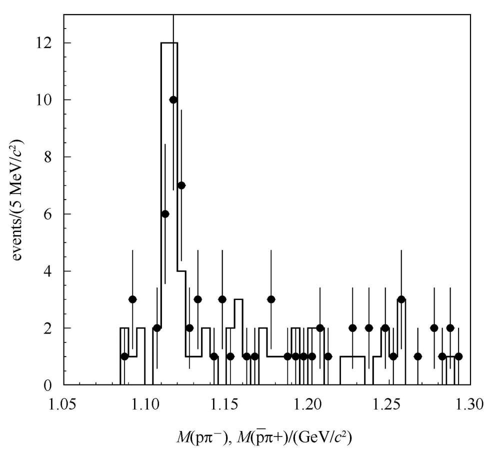

Fig. 2. Comparison of $p\pi^-$ and $\bar{p}\pi^+$ invariant mass distributions (from data). The histogram represents $M_{p\pi^-}$ obtained under the requirements: $|M_{\bar{p}\pi^+}-M_{\bar{\Lambda}}| < 9$ MeV/c^2 and $\chi^2_{4C} < 20$ or $1090 < M_{\bar{p}\pi^+} < 1150$ MeV/c^2 and $\chi^2_{1C} < 10$ whereas the dots with error bars represent $M_{\bar{p}\pi^+}$ obtained under the requirements $|M_{p\pi^-}-M_\Lambda| < 9$ MeV/c^2 and $\chi^2_{4C} < 20$ or $1090 < M_{p\pi^-} < 1150$ MeV/c^2 and $\chi^2_{1C} < 10$. Background seen is mainly from $\psi(2S)\to\Lambda\bar{\Lambda}\phi(1020)$, where $\phi(1020)\to K^+K^-$.

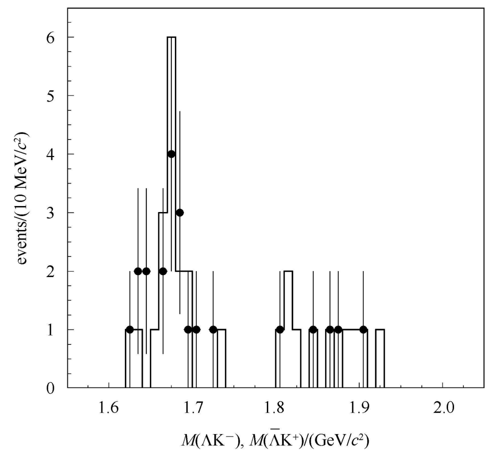

Fig. 3. Comparison of ΛK^- and $\bar{\Lambda}K^+$ invariant mass distributions (from data). The histogram represents $M_{\Lambda K^-}$ obtained under the requirements: $|M_{p\pi^-}-M_\Lambda| < 9$ MeV/c^2 and $|M_{\bar{p}\pi^+}-M_{\bar{\Lambda}}| < 9$ MeV/c^2 and $|M_{\bar{\Lambda}K^+}-M_{\bar{\Omega}^+}| < 15$ MeV/c^2 and $\chi^2_{4C} < 20$ or $1090 < M_{p\pi^-} < 1150$ MeV/c^2 and $1090 < M_{\bar{p}\pi^+} < 1150$ MeV/c^2 and $1630 < M_{\bar{\Lambda}K^+} < 1750$ MeV/c^2 and $\chi^2_{1C} < 10$, and the dots with error bars represent $M_{\bar{\Lambda}K^+}$ obtained under the requirements: $|M_{p\pi^-}-M_\Lambda| < 9$ MeV/c^2 and $|M_{\bar{p}\pi^+}-M_{\bar{\Lambda}}| < 9$ MeV/c^2 and $|M_{\Lambda K^-}-M_{\Omega^-}| < 15$ MeV/c^2 and $\chi^2_{4C} < 20$ or $1090 < M_{p\pi^-} < 1150$ MeV/c^2 and $1090 < M_{\bar{p}\pi^+} < 1150$ MeV/c^2 and $1630 < M_{\Lambda K^-} < 1750$ MeV/c^2 and $\chi^2_{1C} < 10$. Main background channel is $\psi(2S)\to\Lambda\bar{\Lambda}\phi(1020)$, with $\phi(1020)\to K^+K^-$.

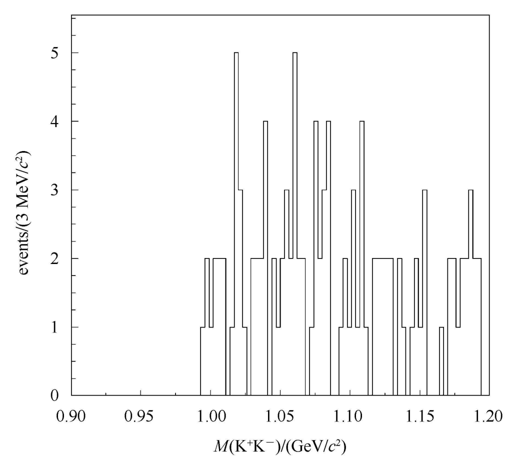

Fig. 4. K^+K^- invariant mass spectrum (for data events) under the constraints: $\chi^2_{1C} < 10$ and $1090 < M_{p\pi^-} < 1150$ MeV/c^2 and $1090 < M_{\bar{p}\pi^+} < 1150$ MeV/c^2.

The number of signal and background events are determined from the scatter plot of $M_{\Lambda K^-}$ versus

$M_{\bar{\Lambda}K^+}$ by employing the technique used in Ref. [8]. For 4C fit events, the scatter plot is obtained under the requirements $|M_{p\pi^-} - M_\Lambda| < 9$ MeV/c^2 and $|M_{\bar{p}\pi^+} - M_{\bar{\Lambda}}| < 9$ MeV/c^2 and $\chi^2_{4C} < 20$ (Fig. 5). In this scatter plot, the signal region is defined by a circle with center at (1672 MeV/c^2, 1672 MeV/c^2) and radius of 15 MeV/c^2. In this region, only one event is found. In this case, the detection efficiency is determined to be 1.62%. Assuming that the observed events follow the Poisson probability distribution [9]:

$$P(x,U) = \frac{e^{-U}U^x}{x!},$$

where x is the number of observed events in an experiment (in this case $x = 1$) and U is the expected number of events, an upper limit for the expected number of events is determined to be $U = 3.89$ at the 90% confidence level.

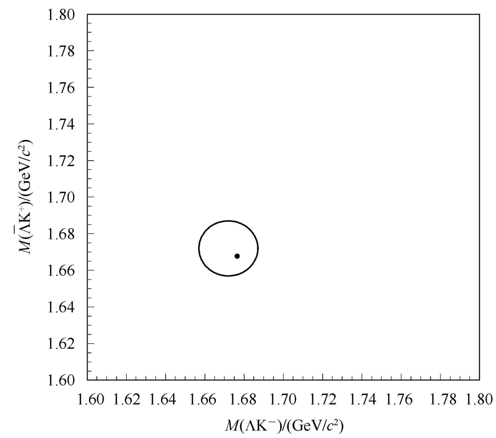

Fig. 5. Scatter plot of ΛK^- versus $\bar{\Lambda}K^+$ for 4C fit events under the constraints: $|M_{p\pi^-} - M_\Lambda| < 15$ MeV/c^2 and $|M_{\bar{p}\pi^+} - M_{\bar{\Lambda}}| < 15$ MeV/c^2 and $\chi^2_{4C} < 20$. The circle with center: (1672 MeV/c^2, 1672 MeV/c^2) and radius of 60 MeV/c^2 represents the signal region.

For 1C fit events, the scatter plot is obtained under the requirements $1090 < M_{p\pi^-} < 1150$ MeV/c^2 and $1090 < M_{\bar{p}\pi^+} < 1150$ MeV/c^2 and $|M(K^+K^-) - M(\phi(1020))| > 15$ MeV/c^2 and $\chi^2_{1C} < 10$ (Fig. 6). In this case the signal region is defined by a circle with center at (1690 MeV/c^2, 1690 MeV/c^2) and radius of 60 MeV/c^2. Two concentric circles of 120 MeV/c^2 and 180 MeV/c^2 radii are used for background estimation in the signal region.

The center of these circles is shifted from nominal central mass value (1672 MeV/c^2) of Ω^- ($\bar{\Omega}^+$) due to the asymmetric nature of the ΛK^- ($\bar{\Lambda}K^+$) invariant mass distribution. The numbers of events found in the signal and background regions are 12 and 6, respectively. So the number of $\Omega^-\bar{\Omega}^+$ signal events is determined to be $12 - 6/5 = 10.8 \pm 3.5$, where 5 is the normalization factor (area of the background region/area of signal region), and the error is statistical. In this case, the detection efficiency is determined to be 8.55%. The significance of the $\Omega^-\bar{\Omega}^+$ signal is obtained to be 3.1σ by using the method described in Ref. [9].

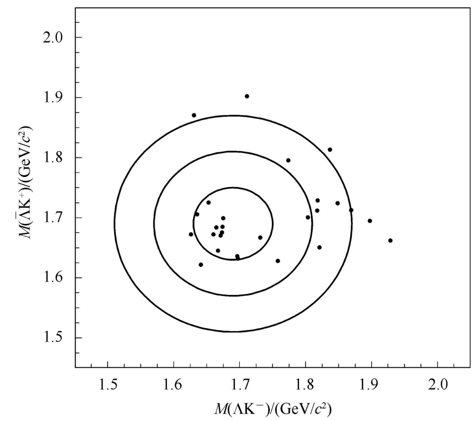

Fig. 6. Scatter plot of ΛK^- versus $\bar{\Lambda}K^+$ for 1C fit events under the constraints: $|M(K^+K^-) - 1020)| > 15$ MeV/c^2 and $1090 < M_{p\pi^-} < 1150$ MeV/c^2 and $1090 < M_{\bar{p}\pi^+} < 1150$ MeV/c^2 and $\chi^2_{1C} < 10$. Circles are centered at (1690 MeV/c^2, 1690 MeV/c^2) due to asymmetric mass limits of Ω^- and $\bar{\Omega}^+$: (1630–1750) MeV/c^2, with radii of 60 MeV/c^2, 120 MeV/c^2 and 180 MeV/c^2. The innermost circle represents the signal region, and the region between the outer circles is used to estimate the normalized background in the signal region.

5 Systematic error analysis

Uncertainties in the branching fraction are studied for 4C and 1C kinematic fit results. The uncertainties of the hadronic interaction model are determined to be 23.3% and 13.2%, respectively, by comparing the numbers of $\Omega^-\bar{\Omega}^+$ MC events reconstructed using the GCALOR and FLUKA models. Particle identification uncertainties are taken as 6% and 5% [6], respectively. MDC tracking errors are taken as 12% and 10% [6], respectively. Kinematic fit uncertainties are 19.1% and 14.6%, respectively, by studying $J/\psi \to \Xi^-\bar{\Xi}^+$ ($\Xi^- \to \Lambda\pi^-$, $\Lambda \to p\pi^-$ and $\bar{\Xi}^+ \to \bar{\Lambda}\pi^-$, $\bar{\Lambda} \to \bar{p}\pi^+$) decays with and without the kinematic fits. Comparing MC $\Omega^-\bar{\Omega}^+$ signal under different values of the angular distribution parameter: $\alpha = 0.5$, $+1$ &-1 with that from the nominal value $\alpha = 0$, the uncertainties are 16.7% and 14.0%, respectively. Monte Carlo statistical errors are evaluated to be 3.6% and 1.5%. The uncertainty due to intermediate branching fractions is 2.4% (by combining the errors in the branching fractions of intermediate resonances [7]) for both the 4C and 1C events. The uncertainty in the number of $\psi(2S)$ data events is 4.3% [10]. Combining all uncertainties in quadrature, the uncertainties for 4C and 1C fit results, are 37.4% and 27.1%, respectively. These results are also listed in Table 1.

Table 1. Systematic uncertainties (%) in the Branching Fraction.

source of uncertainty	4C fit uncertainty	1C fit uncertainty
models of Hadron Interaction	23.3	13.2
particle identification	6	5
MDC tracking	12	10
kinematic fit	19.1	14.6
angular distribution	16.7	14
MC statistics	3.6	1.5
intermediate branching fractions	2.4	2.4
total number of $\psi(2S)$ events	4.3	4.3
	total = 37.4	total = 27.1

6 Determination of branching fraction

Using the following formula:

$$\frac{N^{\rm upper}/(1-\sigma_{\rm sys})}{\epsilon.[B(\Omega^-\to\Lambda{\rm K}^-)]^2.[B(\Lambda\to{\rm p}\pi^-)]^2.N_{\psi(2S)}},$$

where $N^{\rm upper}=3.89$, $B(\Omega^-\to\Lambda{\rm K}^-)=(67.8\pm0.7)\%$ [7], $B(\Lambda\to{\rm p}\pi^-)=(63.9\pm0.5)\%$ [7], $N_{\psi(2S)}=(14\pm0.6)\times10^6$ (number of $\psi(2S)$ data events) [10], $\epsilon=0.0162$ and $\sigma_{\rm sys}=0.374$, an upper limit for the branching fraction of $\psi(2S)\to\Omega^-\bar{\Omega}^+$ is determined to be 1.5×10^{-4} at the 90% confidence level, for 4C fit events. Using the formula:

$$\frac{N^{\rm obs}}{\epsilon.[B(\Omega^-\to\Lambda{\rm K}^-)]^2.[B(\Lambda\to{\rm p}\pi^-)]^2.N_{\psi(2S)}},$$

where $N^{\rm obs}=10.8\pm3.5$ and $\epsilon=0.0855$, the branching ratio is determined to be $(4.80\pm1.56({\rm stat})\pm1.30({\rm sys}))\times10^{-5}$ for 1C fit events. In the limit of $SU(3)$ flavor symmetry, the phase-space-corrected reduced branching fraction ($|M|^2$) for $\psi(2S)\to\Omega^-\bar{\Omega}^+$ is calculated by using the following formula [3]:

$$|M|^2=\frac{B(\psi(2S)\to\Omega^-\bar{\Omega}^+)}{\pi p^*/\sqrt{s}},$$

where p^* is the momentum of Ω^- or $\bar{\Omega}^+$ in $\psi(2S)$ rest frame. In Fig. 7, the reduced branching fraction for $\psi(2S)\to\Omega^-\bar{\Omega}^+$ is plotted along with other octet baryon-antibaryon pairs computed by using the branching fractions from Particle Data Group 2012 [7]. The plot shows a trend towards smaller values of reduced branching fractions for baryon-antibaryon pairs of higher masses.

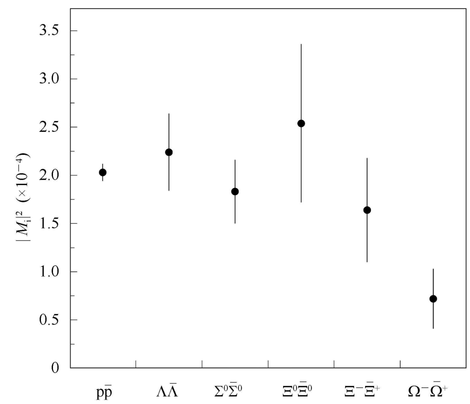

Fig. 7. The reduced branching fractions: $|M_{\rm i}|^2= B(\psi(2S)\to{\rm B_i\bar{B}_i})/(\pi p^*/\sqrt{s})$, where p^* is momentum of baryon (antibaryon) in rest frame of $\psi(2S)$.

7 Conclusion

Using 14 million $\psi(2S)$ decay events recorded by the BESⅡ detector at BEPC, we report an upper limit for the branching fraction of $\psi(2S)\to\Omega^-\bar{\Omega}^+$ to be 1.5×10^{-4} at 90% confidence level based upon the 4C fit result. We report the first evidence of an $\Omega^-\bar{\Omega}^+$ signal, with a statistical significance of about 3.1σ using 1C events. The branching fraction of $\psi(2S)\to\Omega^-\bar{\Omega}^+$ is determined to be $(4.80\pm1.56({\rm stat})\pm1.30({\rm sys}))\times10^{-5}$ and is consistent with the upper limit.

The BES Collaboration would like to thank the staff of BEPC and the Computing Center for their hard work.

References

1 Farrar G R, Jackson R D. Phys. Rev. Lett., 1975,**35**: 1416; Ioffe B L. Phys. Lett. B, 1976, **63**: 425; Vainshtein A I, Zakharov V I. Phys. Lett. B, 1978, **72**: 368; Brodsky S J, Lepage G P. Phys. Rev. D, 1981, **24**: 2848

2 Bolz J. Kroll P. Eur. Phys. J. C, 1998, **2**: 545–556

3 BAI J Z et al. (BES collaboration). Phys. Rev. D, 2001, **63**: 032002

4 Pedlar T K et al. (CLEO collaboration). Phys. Rev. D, 2005, **72**: 051108

5 BAI J Z et al. (BES collaboration). Nucl. Instrum. Methods A, 2001, **458**: 627

6 Ablikim M et al. (BES collaboration). Nucl. Instrum. Methods A, 2005, **552**: 344

7 Beringer J et al. (Particle Data Group). Phys. Rev. D, 2012, **86**: 010001 (web edition: accessed on July 09, 2012)

8 Ablikim M et al. (BES collaboration). Phys. Rev. D, 2004, **70**: 092002

9 Bityukov S I, Krasnikov N V. Nucl. Instrum. Methods A, 2003, **502**: 795–798

10 Ablikim M et al. (BES collaboration). Phys. Lett. B, 2007, **648**: 149–155